ACS OMEGA

Open Access

http://pubs.acs.org/journal/acsodf

Article

Design, Synthesis, and Antirheumatoid Arthritis Mechanism of TLR4 Inhibitors

Shiyang Zhou,* Weiwei Xue,* and Jun Tan*

Cite This: *ACS Omega* 2024, 9, 36232−36241

Read Online

ACCESS | Metrics & More | Article Recommendations

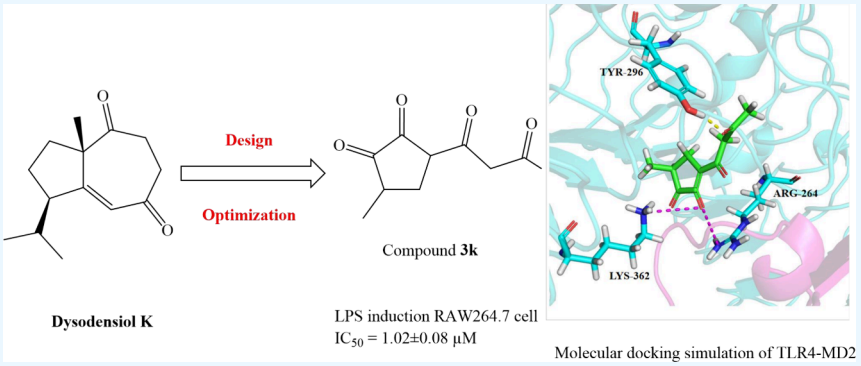

ABSTRACT: A total of 12 carbonyl compounds were synthesized, their lipopolysaccharide induced inhibition, and activity of RAW264.7 cells was evaluated. The most active compound **3k** inhibited RAW264.7 cells with IC_{50} value of 1.02 ± 0.08 μM. Compound **3k** significantly inhibited the release of TNF-α, IL-1β, and IL-6 in supernatant for RAW264.7 cells. In vivo collagen-induced arthritis model tests administered orally, compound **3k** showed effects similar to those of methotrexate in the positive control group. The preliminary mechanism study showed that compound **3k** had an effect on abnormal expression for TLR4, TNF-α, NF-κB protein, and genes related to inflammation signaling pathway in RAW264.7 cells. Meanwhile, compound **3k** showed a good affinity for the TLR4 receptor in molecular docking simulation. Therefore, compound **3k** may be a promising lead compound for the treatment of rheumatoid arthritis.

1. INTRODUCTION

Rheumatoid arthritis (RA) is an immune disease characterized by inflammation of the synovial membrane and mainly affects joints.[1−3] RA seriously affects human health and quality of life; the prevalence rate of the world population is 0.5−1%, and many countries have listed RA as one of their national key diseases.[4] The main clinical manifestation for RA patients is synovitis; symptoms of joint pain, deformity, and loss of function will occur in patients with continued progression of the disease; and severe cases will lead to death. Reducing joint inflammation and joint pain has been the main goal for RA treatment.[5−7] As far as possible, efforts are made to protect the functions for muscles and joints and to achieve the purpose of complete remission or reduction for disease activity, thereby improving the overall function of the patient.[8−10] The etiological pathogenesis of RA is very complex, and the results of modern medical research show that the onset of rheumatoid arthritis may be related to a variety of receptors, such as toll-like receptor 4 (TLR4), α tumor necrosis factor (TNF-α), nuclear factor κB (NF-κB), non-receptor tyrosine protein kinase 2 (JAK2), and signal transduction and transcriptional activator 3 (STAT3).[11−14] TLR4 plays an important role in activating an innate immune response by directly recognizing pathogene-associated molecular patterns,[15,16] including lipopolysaccharide (LPS), lymphotoxin-α (LT-α), and double-stranded ribonucleic acid (dsRNA).[17] At present, there is no effective cure for RA, and clinical use of antirheumatic drugs can inhibit the development of the disease, but there are also some drawbacks such as drug toxicity, affects on immunity, and a high treatment price.[18] For example, the anti-RA-activity IC_{50} such as methotrexate is generally at the micromolar level, and there are toxic side effects such as nausea, vomiting, and stomatitis.[19−22] In view of the current clinical deficiencies of RA drugs, it was of great significance to find new inhibitors for RA and development of new therapeutic strategies.[23−25]

Received: March 10, 2024
Revised: July 12, 2024
Accepted: July 24, 2024
Published: August 14, 2024

Fissistigma oldhami (*F. oldhami*) is distributed in China and Vietnam and grows in the waterside shrubs of low-elevation valleys.[26−30] The stem and skin fibers of guapeng wood can be woven into twine, sacks, and paper making; the flower can be used to extract oil or extract the melon fumu flower, used as raw materials for cosmetics and soap; seed oil is used for industrial oil and cosmetics. The root can be used as a kind of Chinese medicine used to treat injuries and arthritis. Some researchers studied the chemical components of *F. oldhami*, isolated a variety of monomers, and screened these monomers for their anti-RA activity in vitro. Some of the compounds showed a good inhibitory effect on synovium cells.[31−33] The inhibitory activity of Dysodensiol K for synovial cells was $IC_{50} = 11.8 \pm 0.23\ \mu M$, in vitro. In previous studies,[34−36,42] the lead compound Dysodensiol K was taken as the skeleton structure, and on this basis, structural modification were carried out, and some research results have been obtained. In this study, further structural transformation of Dysodensiol K was carried out, and a total of 12 target compounds were designed (Figure 1). In this study, we

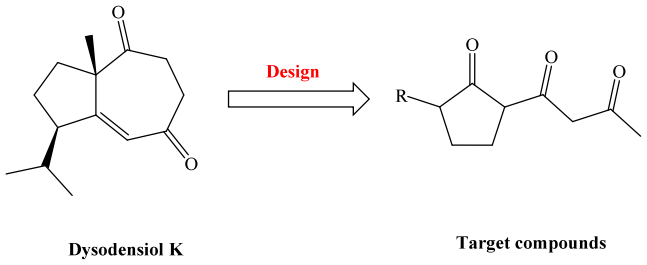

Figure 1. Structural design of target compounds **3a−3l**.

described the synthesis of novel carbonyl compounds and evaluated the antirheumatoid arthritis activity of the derivatives.[34−36] In this study, the target compounds with antirheumatoid arthritis were screened through in vitro and in vivo activity evaluation. On this basis, the binding of these compounds to receptors was further studied to elucidate the mechanism of their antirheumatoid arthritis action. These studies provide a certain experimental basis for promoting the research for carbonyl compounds against RA.

2. RESULTS AND DISCUSSION

2.1. Design and Chemical Synthesis. Chemical structure analysis for Dysodensiol K showed that it had a carbonyl structure. Therefore, we propose that the carbonyl structure may be the group of compounds with antirheumatoid arthritis active groups. In previous studies,[34−36] closed-loop carbonyl compounds were synthesized, while open-loop carbonyl compounds as intermediates have not received much attention. Based on the previous research results,[34,36] we believe that open-ring carbonyl compounds may also have good antirheumatoid arthritis activity. Recent studies[42] have shown that carbonyl compounds with open-ring structure (six-membered parent nuclei) exhibit excellent antirheumatoid arthritis activity. Therefore, along with the existing research results, we further optimized the lead compounds and designed and synthesized the open-ring carbonyl compounds with the five-membered ring as the parent nucleus. In this study, we designed and synthesized carbonyl compounds **3a−3l** with a similar parent nuclear structure using Dysodensiol K as the lead compound (Figure 1). The target compounds **3a−3l** were synthesized according to the method we reported earlier[36,42] (Scheme 11). In the one-step synthesis reaction, *p*-TsOH was used as catalyst, the yield was 99%, and the product (compound **2a**) after reaction can be directly used as raw material for further reaction without purification. In the second-step, the yield of the final product (compounds **3a−3l**) was 79.1%−91.3% with sodium ethanol as the basic substance.

2.2. Inhibitory Rate of RAW 264.7 Cells and the Effect of Inflammatory Factors In Vitro. As inflammatory and immune diseases, the pro-inflammatory cytokines IL-6, IL-1β, and TNF-α in pathogenesis for RA play a role in regulating the apoptosis of synovial cells. The inhibitory activity for target compounds against LPS-induced RAW264.7 cells was used as an index to evaluate the antirheumatoid arthritis activity, in vitro.[20−22] Methotrexate was used as the positive control group, LPS as the model group, and dimethyl sulfoxide (DMSO) as the blank control group in the in vitro activity determination. Compared with the normal group (100.00 ± 2.03%), the cell survival rate of the model group (185.18 ± 6.41%) was significant increased. Compared with the model group, RAW 264.7 cells in DMSO group had no obvious growth inhibition. The results of biological activity in vitro showed that designed target compounds **3a−3l** could inhibit activity for RAW264.7 cells with IC_{50} values of 1.02−6.13 μM (Table 1). The tested target compounds were basically at the same level as the positive control group ($IC_{50} = 1.21 \pm 0.13\ \mu M$), in which the target compounds **3a**, **3g**, **3h**, **3i**, **3j**, and **3k** showed relatively good activity, and their inhibitory activity IC_{50} on LPS induction RAW264.7 cells were 2.91 ± 0.24, 1.61 ± 0.09, 1.94 ± 0.13, 1.73 ± 0.15, 2.45 ± 0.20, and 1.02 ± 0.08 μM, respectively. On the basis of this, we further measured the effect of the target compounds **3a**, **3g**, **3h**, **3i**, **3j**, and **3k** on the inflammatory factor level of RAW264.7 cells (Table 2). The results of in vitro activity determination showed that levels for inflammatory factors TNF-α, IL-1β, and IL-6 in RAW264.7 cells supernatant for the model group were significantly increased. The levels for inflammatory factors TNF-α, IL-1β, and IL-6 in RAW264.7 cells supernatant for the DMSO group has no significant change, while levels for inflammatory factors TNF-α, IL-1β, and IL-6 in RAW264.7 cells supernatant for the 1 μM methotrexate positive group was significantly decreased. Contents for TNF-α, IL-1β, and IL-6 in

Scheme 1[a]

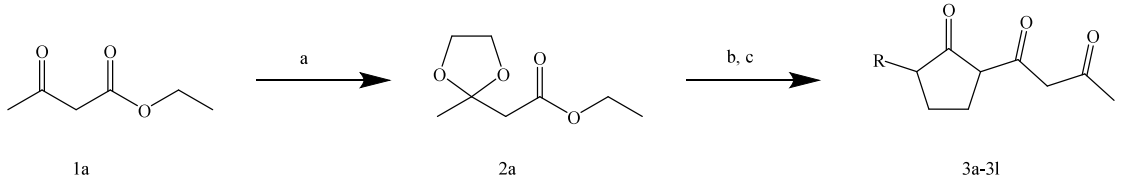

[a]Reaction conditions: (a) ethylene glycol, benzene, and *p*-TsOH, reflux 24 h; (b) substituted cyclopentanone, C_2H_5OH, and C_2H_5ONa, reflux 12 h; (c) HCl and H_2O, 30 °C, 1 h.

https://doi.org/10.1021/acsomega.4c02344
ACS Omega 2024, 9, 36232−36241

Table 1. In Vitro Inhibition Activity of the RAW 264.7 Cells

Compounds	Structure	$IC_{50} \pm SD$ (μM)[a]
3a	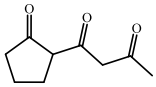	2.91±0.24
3b	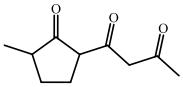	3.45±0.31
3c	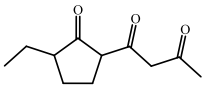	3.55±0.32**
3d	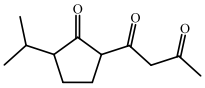	4.03±0.41
3e	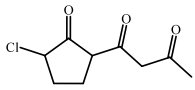	3.59±0.26
3f	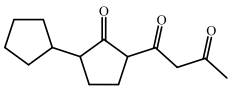	3.31±0.29
3g	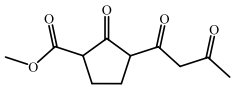	1.61±0.09**
3h	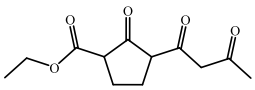	1.94±0.13
3i	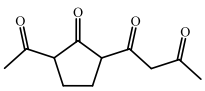	1.73±0.15
3j	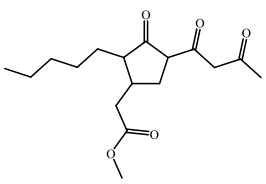	2.45±0.20
3k	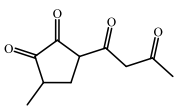	1.02±0.08**
3l	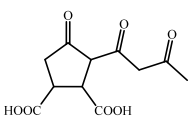	6.13±0.42
methotrexate[b]	—	1.21±0.13
model	—	185.18±6.41% (survival rate)
normal	—	100.00±2.03% (survival rate)
DMSO	—	3.43±1.78 % (inhibition rate)

[a]Average of three independent experiments. Values marked with **: compared with normal group , $p < 0.01$. [b]Positive control.

supernatant for RAW 264.7 cells in the 1 μM target compounds group were also significantly decreased to varying degrees, and compound **3k** had the best inhibition effect on release for TNF-α, IL-1β, and IL-6. These results suggested that compound **3k** could effectively inhibit proliferation for RAW 264.7 cells by LPS induction and significantly inhibit the release for inflammatory cytokines TNF-α, IL-1β, and IL-6 in a supernatant of RAW 264.7 cells, and compound **3k** had the best effect. The specific mechanism of TNF-α, IL-1β, and IL-6 related signaling pathways will be further revealed.

2.3. In Vivo Biological Activity. Combined with in vitro activity results, compound **3k** was necessary for activity testing in vivo. In a rat CIA (collagen-induced arthritis) model, we evaluated therapeutic effects for compound **3k**, including paw volume and TNF-α and IL-6 concentrations. In paw volume evaluation for rats (Figure 2), the experimental results showed that the paw volume of rats treated with a high dose of compound **3k** (100 (mg/kg)/day) was basically unchanged. However, the paw volume of rats treated with a low dose of compound **3k** (50 (mg/kg)/day) was also basically unchanged. In Figure 3 (50 (mg/kg)/day), the model group (Figure 3b) showed obvious redness and swelling, and the claw light was enlarged. After the treatment of compound **3k** (Figure 3d), the rat's claws were not red and swollen, and the size of the paws was almost the same. The results of serum IL-6 and TNF-α concentrations in rats showed that the target compound **3k** could improve inflammation at both high and low doses (Figure 4). As can be seen from Figure 4, IL-6 and TNF-α concentrations in the model group were significantly higher than those in the blank group, indicating successful modeling. Compared with the model group, after treatment with compound **3k**, serum IL-6 and TNF-α concentrations decreased significantly and reached the normal level, indicating that compound **3k** inhibits inflammatory factors IL-6 and TNF-α, thus achieving the therapeutic effect. In in vivo animal models, the activity of open-ring compounds was improved compared with previous studies,[34,36] which suggests that this type of compound may be easier to bind to receptors, thus achieving anti-inflammatory and other activities.

2.4. Mechanism of Action against Rheumatoid Arthritis. The mechanism of drug action was the theory explaining how or why a drug acts, which is an important part of pharmacodynamics. In order to elucidate the antirheumatoid arthritis mechanism of carbonyl compounds, combined with in vitro and in vivo activity results, compound **3k** was selected as the representative for related studies (Figures 5−7).

Immunofluorescence analysis showed (Figure 5) that expressions for inflammatory signaling pathway related proteins TLR4, TNF-α, and NF-κB of RAW264.7 cells in the model group were significantly increased ($p < 0.01$). The expressions for TLR4, TNF-α, and NF-κB proteins of RAW264.7 cells at 1 μM methotrexate group were significantly down-regulated ($p < 0.01$). Expressions for TLR4, TNF-α, and NF-κB of RAW264.7 cells were significantly down-regulated with 1 μM compound **3k** treatment ($p < 0.05$). Western blot assay showed (Figure 6) that expressions for inflammatory signaling pathway related proteins TLR4, TNF-α, and NF-κB of RAW264.7 cells in the model group were significantly increased ($p < 0.01$). Expressions for TLR4, TNF-α, and NF-κB proteins of RAW264.7 cells in the 1 μM methotrexate group was significantly down-regulated ($p < 0.01$). Expressions of TLR4, TNF-α, and NF-κB for RAW264.7 cells were significantly down-regulated with 1 μM compound **3k** treatment ($p < 0.05$). RT-PCR results showed (Figure 7) that expressions for genes related to inflammation signaling pathways TLR4, TNF-α, and NF-κB for RAW264.7 cells in the model group were significantly up-regulated ($p < 0.01$). Expressions for TLR4, TNF-α, and NF-κB genes of RAW264.7 cells in the 1 μM methotrexate group were significantly down-regulated ($p < 0.01$). Expressions for TLR4, TNF-α, and NF-κB genes of RAW264.7 cells were significant down-regulated with 1 μM compound **3k** treatment ($p < 0.05$). Compound **3k** had a better

https://doi.org/10.1021/acsomega.4c02344
ACS Omega 2024, 9, 36232−36241

Table 2. Determination of the Level of Inflammatory Factors of RAW264.7 Cells

Group	Concn	Inflammatory factor (pg/L)[a]		
		TNF-α	IL-1β	IL-6
normal		179.8 ± 35.5	201.8 ± 9.0	88.6 ± 10.8
model		656.8 ± 71.3##	667.3 ± 81.4##	232.7 ± 25.7
DMSO	5‰	538.3 ± 44.9	572.7 ± 29.8	180.5 ± 32.1
methotrexate[b]	1 μM	236.8 ± 18.7**	337.6 ± 47.8**	114.1 ± 2.8**
3a	1 μM	520.6 ± 54.6	512.0 ± 85.0	196.2 ± 14.3
3g	1 μM	339.8 ± 49.2**	408.2 ± 69.1**	170.3 ± 25.3**
3h	1 μM	524.7 ± 48.5	506.0 ± 65.1	197.4 ± 21.3
3i	1 μM	424.5 ± 87.6*	558.4 ± 66.9	205.2 ± 25.9
3j	1 μM	400.6 ± 60.2**	488.8 ± 66.1*	163.8 ± 25.9*
3k	1 μM	217.8 ± 20.3**	278.6 ± 58.1*	96.6 ± 9.8**

[a]The average of three independent experiments. Compared with normal group ## was $p < 0.01$; compared with model group * was $p < 0.05$ and ** was $p < 0.01$. [b]Positive control.

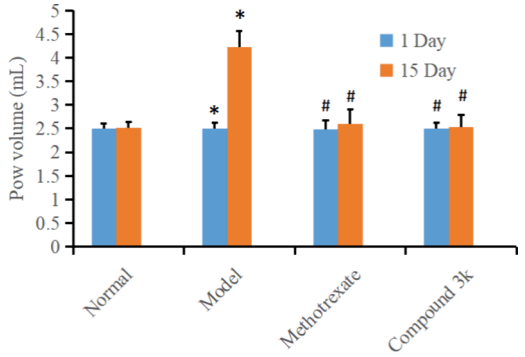

Figure 2. Rat paw volume. Compared with normal group, * was $P < 0.05$; compared with model group, # was $P < 0.01$.

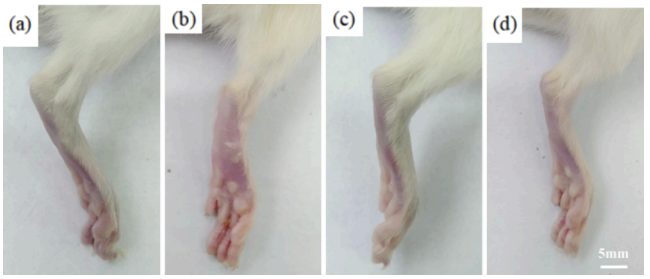

Figure 3. In low doses, the rats paw volume was a physical figure. (a) Normal group; (b) model group; (c) methotrexate group; (d) compound **3k** group. Dose of 50 (mg/kg)/day.

effect on down-regulation for TLR4, TNF-α, and NF-κB genes. It was also suggested that compound **3k** could regulate the abnormal expression for TLR4, TNF-α, and NF-κB of RAW264.7 cells related to the inflammatory signaling pathway. In conclusion, compound **3k** has an obvious regulator effect on abnormal expressions of TLR4, TNF-α, and NF-κB proteins and genes related to inflammatory signaling pathways of RAW264.7 cells. Among them, compound **3k** has better regulation of the TLR4/TNF-α/NF-κB signal.

2.5. Pharmacokinetics of Compound 3k. To investigate the oral bioavailability of compound **3k**, we performed pharmacokinetic tests in Sprague-Dawley rats (SD rats). When pharmacokinetics were administered intravenously and orally, the amount of drugs in the blood generally tended to decrease and the bioavailability of all species can reach 100% (Figure 8). The half-life of compound **6** in rats at an oral dose of 100 mg/kg was 0.5−1 h, reaching a maximum concentration of 2014 ng/mL at 0.08 h after administration. The half-life of compound **3k** in rats given an intravenous dose of 20 mg/kg was also in a small time frame of 0.5−1 h. The maximum concentration reached 1603 ng/mL at 0.11 h after administration. In pharmacokinetic (PK) experiment studies in SD rats, compound **3k** showed superior drug exposure.

2.6. Molecular Docking Simulation of Compound 3k with TLR4-MD-2. In order to gain a better understanding of the binding mode between target compound **3k** and TLR4 through molecular docking, the model for TLR4-MD-2 induced by LPS was chosen as receptor. The binding pocket of the receptor

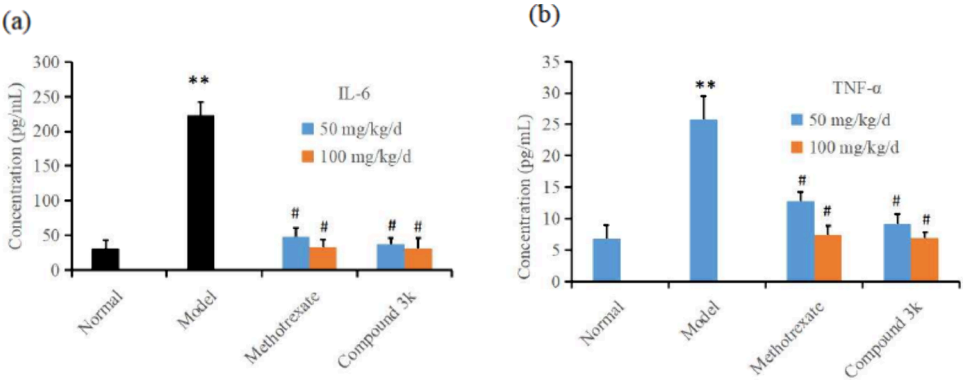

Figure 4. IL-6 and TNF-α concentrations. (a) Dose was 50 (mg/kg)/day; (b) dose was 100 (mg/kg)/day. Compared with normal group ** was $p < 0.01$; compared with model group # was $p < 0.01$.

https://doi.org/10.1021/acsomega.4c02344
ACS Omega 2024, 9, 36232−36241

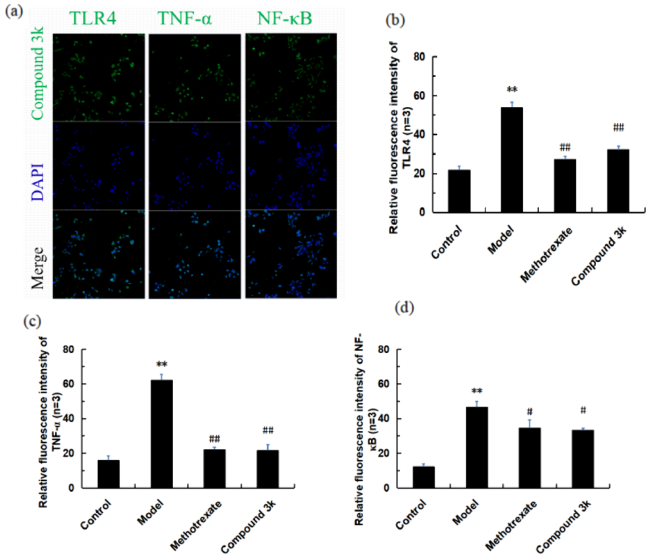

Figure 5. Expressions and quantitative analyses of TLR4, TNF-α, and NF-κB proteins in RAW264.7 cells by immunofluorescence. (a) Immunofluorescence for TLR4, TNF-α and NF-κB protein expression (200 ×); (b) quantitative analysis for TLR4 protein; (c) quantitative analysis for TNF-α protein; and (d) quantitative analysis for NF-κB protein. Compare with normal group ** was $p < 0.01$; compared with model group # was $p < 0.01$.

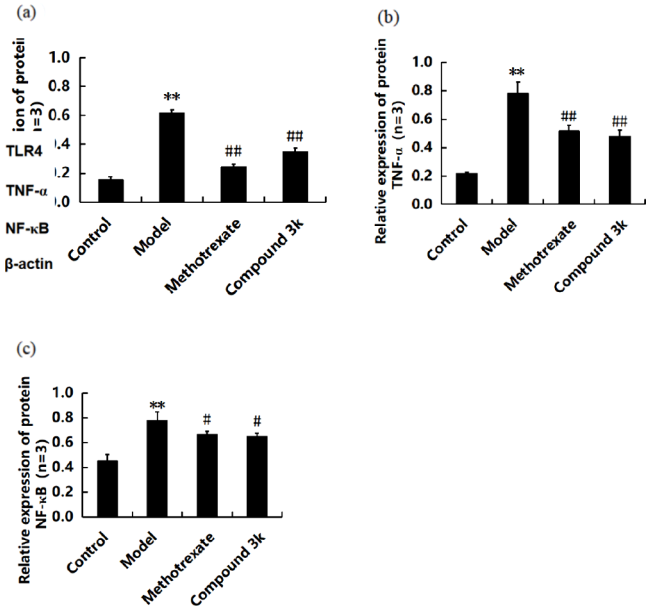

Figure 6. Expressions and quantitative analyses for TLR4, TNF-α and NF-κB proteins of RAW264.7 cells by Western blot: (a) expression for TLR4 protein; (b) expression for TNF-α protein; (c) Expression for NF-κB protein. Compare with normal group ** was $P < 0.01$, compare with model group # was $P < 0.01$ and ## was $P < 0.05$.

consists of two parts. One consists of hydrophobic residues for MD-2 with unsaturated and saturated fatty acid chains. The other one consists of partial interface residues for TLR4 which prefer combined carbonyl group and aromatic ring. As the target compounds contain a carbonatic ring, the latter binding pocket was chosen for the docking study. As was shown in Figure 9, compound **3k** forms one H-bond with TYR 296 and two salt bridges with LYS 362 and ARG 264. Compared with the results of previous studies,[34,36] in molecular docking, the dicarbonyl

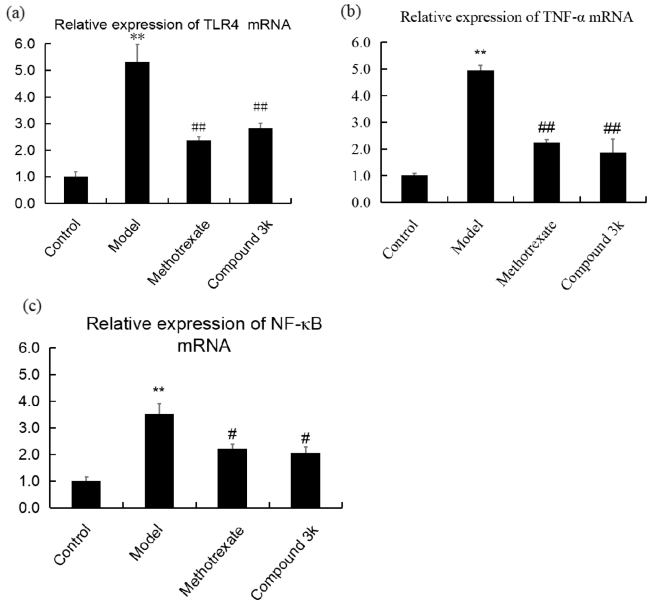

Figure 7. mRNA expressions for TLR4, TNF-α, and NF-κB proteins of RAW264.7 cells.

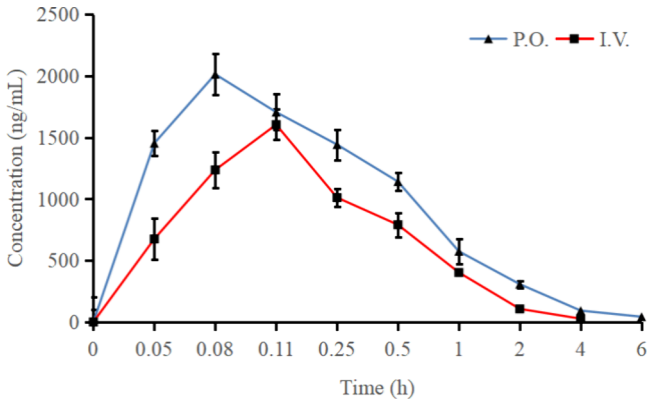

Figure 8. Plasma concentrations after the oral and intravenous administration of compound **3k**.

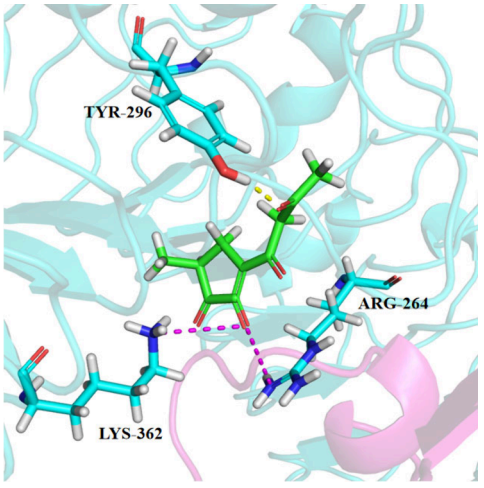

Figure 9. Binding modes between TLR4-MD2 and compound **3k**.

chain and TLR4 receptor residues in the open-ring target compound were changed, and the residues of the five-membered ring structure fragment and the receptor were all ARG 264,

https://doi.org/10.1021/acsomega.4c02344
ACS Omega 2024, 9, 36232−36241

which may lead to the difference between the open-ring and nonopen-ring compounds in the resistance to rheumatoid arthritis. In addition, the docking score of the optimal conformations of compound **3k** was −3.47 kcal/mol. To sum up, the hydrogen bonding formed between the carbonyl groups of compound **3k** and chain of residues, and the electrostatic interactions were the predominant forces for ligand recognition and to make small molecules tightly bind to TLR-MD-2.

3. CONCLUSION

In this report, a total 12 of 1-(2-oxocyclopentyl) butane-1, 3-dione derivatives was synthesized as the new antirheumatoid arthritis drugs. The biological activity evaluation showed that compound **3k** (IC_{50} = 1.02 ± 0.08 μM) had better inhibitory activity than positive control (methotrexate, IC_{50} = 1.21 ± 0.13 μM). Of note, compound **3k** was further tested for its effect on levels of inflammatory cytokines for RAW264.7 cells. We found that levels of TNF-α, IL-1β, and IL-6 of compound **3k** were better than those of the positive control at the same concentration. In vivo, compound **3k** exhibited an effect similar to that of the positive control group methotrexate. The mechanism study showed that compound **3k** had an effect on abnormal expression for TLR4, TNF-α, and NF-κB proteins and genes. At the same time, the molecular docking study found that compound **3k** had a good affinity for the TLR4 associate with RA. These results showed that compound **3k** was further studied to enable them to serve as candidates for antirheumatoid arthritis.

4. EXPERIMENTAL PART

4.1. Synthesis Experiment. The purity of the final compound was determined by HPLC to be >95%. ^{1}H NMR and ^{13}C NMR spectra were recorded by Bruker AVANCE NEO 400 MHz (Sanshu Biotech. Co., Ltd., Shanghai, China). The target compounds **3a**−**3l** were synthesized according to the method we reported earlier.[36,42]

*4.1.1. Synthesis of Compound **2a**.* The 13.01 g amount of ethyl acetoacetate (compound **1a**, 100 mmol) and 5.58 mL of ethylene glycol (100 mmol) were accurately weighed in 250 mL of dry round-bottom flasks. A 150 mL portion of benzene was added to remove water as the reaction solvent, and then an appropriate amount of *p*-methylbenzenesulfonic acid (*p*-TsOH, 0.5% of the substrate) was added as the catalyst. The solvent was slowly heated to boiling, and magnetic stirring of the reflux reaction was continued for 24 h. Upon completion of the reflux reaction, the mixture was vacuum distilled to remove and recover the reaction solvent benzene, yielding the intermediate compound **2a**. Compound **2a** was a colorless liquid with a yield of 98.6%.

*4.1.2. Synthesis of Compounds **3a**−**3l**.* A 17.42 g amount of compound **2a** (100 mmol) and 8.41 g of cyclopentanone (100 mmol) were accurately weighed and placed in 250 mL dry round-bottom flasks. A 150 mL aliquot of absolute ethanol was added as the condensation reaction solvent, and 6.80 g of sodium ethanol (100 mmol) was added as the basic substance after stirring evenly by magnetic force. The solvent was slowly heated to boiling, and magnetic stirring of the reflux reaction was continued for 12 h. When the reflux reaction was completed, the mixture was vacuum distilled to remove and recover reaction solvent ethanol to obtain a viscous residue. A 100 mL aliquot of 1 mol/L HCl was added to residue. After HCl was added, the mixture was placed in a 30 °C water bath for 1 h. After the hydrolysis reaction was completed, the mixture was extracted for 50 mL of ethyl acetate, and the organic layer was collected and washed for saturated sodium bicarbonate ($NaHCO_3$). Finally, the organic layer was dried for anhydrous sodium sulfate (Na_2SO_4), the filtrate was collected by filtration, and filtrate was vacuum distilled to remove ethyl acetate to obtain a crude product mixture (compound **3a**). Crude compound **3a** was purified by silica gel column chromatography (the solvent was ethyl acetate:petroleum ether = 1:4), and the pure product compound **3a** was a oorange-yellow oily liquid. Compounds **3b**−**3l** were synthesized by the same method, and these products were orange-yellow oily liquids.

*1-(2-Oxocyclopentyl)butane-1,3-dione (compound **3a**).* Orange-yellow oily liquid; yield 91.3%. ^{1}H NMR (400 MHz, DMSO-d_6): δ 1.80−2.20 (7H, 1.86 (dt, J = 13.5, 1.4 Hz), 1.91 (dd, J = 13.7, 7.5 Hz), 2.05 (dt, J = 13.5, 5.4 Hz), 2.11 (dd, J = 13.7, 5.4 Hz), 2.15 (s)), 2.33−2.55 (2H, 2.44 (dd, J = 15.2, 1.4 Hz), 2.47 (dd, J = 15.2, 5.5 Hz), 3.56 (2H, s), 3.83 (1H, dd, J = 7.5, 7.0 Hz). ^{13}C NMR (100 MHz, DMSO-d_6): δ 23.7, 29.1, 29.4, 37.9, 56.9, 59.0, 197.8, 200.0, 210.2. HR-ESI-MS m/z. Ccalcd for $C_9H_{12}O_3$\{[M + H]$^+$\}:168.1920. Found: 168.1917. Elem. Anal. Calcd for $C_9H_{12}O_3$: C, 64.27; H, 7.19; O, 28.54. Found: C, 64.26; H, 7.21; O, 28.53%.

*1-(3-Methyl-2-oxocyclopentyl)butane-1, 3-dione (compound **3b**).* Orange-yellow oily liquid; yield 89.2%. ^{1}H NMR (400 MHz, DMSO-d_6): δ 1.15 (3H, s), 1.80−2.32 (7H, 1.89 (dd, J = 13.5, 1.8 Hz), 2.02 (dd, J = 13.5, 5.5 Hz), 2.13 (dd, J = 13.9, 1.4 Hz), 2.17 (s), 2.21 (dd, J = 13.9, 5.4 Hz), 2.40 (1H, dd, J = 6.9, 1.8 Hz), 3.56 (2H, s), 3.69 (1H, dd, J = 9.3, 5.5 Hz). ^{13}C NMR (100 MHz, DMSO-d_6): δ 14,7, 24.5, 29.4, 31.1, 44.3, 56.9, 61.4, 197.3, 200.0, 219.8. HR-ESI-MS m/z. Calcd for $C_{10}H_{14}O_3$\{[M + H]$^+$\}: 182.2190. Found 182.2189. Elem. Anal. Calcd for $C_{10}H_{14}O_3$: C, 65.92; H, 7.74; O, 26.34. Found: C, 65.90; H, 7.74; O, 26.36%.

*1-(3-Ethyl-2-oxocyclopentyl) butane-1,3-dione (compound **3c**).* Orange-yellow oily liquid; yield 87.4%. ^{1}H NMR (400 MHz, DMSO-d_6): δ 1.02 (3H, s), 1.56 (2H, dd, J = 6.9, 4.6 Hz), 1.95 (1H, dd, J = 13.6, 1.4 Hz), 2.09−2.42 (6H), 2.16 (dd, J = 14.1, 5.4 Hz), 2.16 (s), 2.19 (dd, J = 14.1, 5.5 Hz), 2.32 (dd, J = 13.6, 5.5 Hz), 2.65 (1H, dd, J = 7.5, 4.6 Hz), 3.56 (2H, s), 3.75 (1H, dd, J = 5.3, 1.4 Hz). ^{13}C NMR (100 MHz, DMSO-d_6): δ 11.7, 23.5, 25.6, 29.4, 29.6, 51.4, 56.9, 61.7, 197.3, 200.0, 215.1. HR-ESI-MS m/z. Calcd for $C_{11}H_{16}O_3$\{[M + H]$^+$\}:196.2460. Found: 196.2461. Elem. Anal. Calcd for $C_{11}H_{16}O_3$: C, 67.32; H, 8.22; O, 24.46. Found: C, 67.31; H, 8.21; O, 24.48%.

*1-(3-Isopropyl-2-oxocyclopentyl)butane-1,3-dione (compound **3d**).* Orange-yellow oily liquid; yield 85.1%. ^{1}H NMR (400 MHz, DMSO-d_6): δ 0.94 (6H, s), 1.84−2.02 (2H), 1.92 (dd, J = 13.5, 1.4 Hz), 1.94 (dd, J = 6.9, 2.4 Hz), 2.05−2.46 (6H), 2.16 (dd, J = 14.1, 5.4 Hz), 2.19 (dd, J = 14.1, 1.4 Hz), 2.33 (dd, J = 13.5, 5.5 Hz), 2.55 (1H, dd, J = 7.5, 2.4 Hz), 3.56 (2H, s), 3.75 (1H, dd, J = 5.3, 1.4 Hz). ^{13}C NMR (100 MHz, DMSO-d_6): δ 20..4, 26.4, 28.0, 29.0, 29.4, 54.6, 56.9, 61.4, 197.3, 200.0, 211.2. HR-ESI-MS m/z. Calcd for $C_{12}H_{18}O_3$\{[M + H]$^+$\}: 210.2730. Found: 210.2728. Elem. Anal. Calcd for $C_{12}H_{18}O_3$: C, 68.55; H, 8.63; O, 22.83. Found: C, 68.56; H, 8.63; O, 22.82%.

*1-(3-Chloro-2-oxocyclopentyl)butane-1,3-dione (compound **3e**).* Orange-yellow oily liquid; yield 80.3%. ^{1}H NMR (400 MHz, DMSO-d_6): δ 1.84−2.26 (7H), 1.98 (dd, J = 13.7, 5.5 Hz), 2.04 (dd, J = 13.4, 5.4 Hz), 2.09 (dd, J = 13.4, 1.4 Hz), 2.15 (dd, J = 13.7, 1.4 Hz), 2.18 (s), 3.56 (2H, s), 3.79 (1H, dd, J = 7.5, 7.0 Hz), 5.26 (1H, dd, J = 5.3, 1.4 Hz). ^{13}C NMR (100 MHz, DMSO-d_6): δ 27.4, 29.4, 31.9, 56.9, 62.1, 63.8, 197.3, 200.0,

https://doi.org/10.1021/acsomega.4c02344
ACS Omega 2024, 9, 36232−36241

212.9. HR-ESI-MS *m/z*. Calcd for $C_9H_{11}ClO_3$\{[M + H]$^+$\}: 202.6340. Found: 202.6338. Elem. Anal. Calcd for $C_9H_{11}ClO_3$: C, 53.35; H, 5.47; Cl, 17.49; O, 23.69. Found: C, 53.34; H, 5.48; Cl, 17.48; O, 23.70%.

1-(2-Oxo-[1,1′-bi(cyclopentan)]-3-yl)butane-1,3-dione (compound **3f**). Orange-yellow oily liquid; yield 82.4%. ^{1}H NMR (400 MHz, DMSO-d_6): δ 1.45−1.80 (8H), 1.58 (dd, J = 11.9, 5.4 Hz), 1.60 (dd, J = 13.4, 7.0 Hz), 1.63 (dd, J = 14.9, 5.4 Hz), 1.65 (dd, J = 14.9, 1.4 Hz), 1.67 (tt, J = 12.9, 5.3 Hz), 1.71 (dd, J = 11.9, 1.4 Hz), 1.95 (1H, dd, J = 13.6, 1.4 Hz), 2.07−2.48 (7H, 2.16 (dd, J = 14.1, 5.4 Hz), 2.15 (s), 2.20 (dd, J = 14.1, 1.4 Hz), 2.27 (dd, J = 10.2, 4.1 Hz), 2.38 (dd, J = 13.6, 5.5 Hz)), 2.62 (1H, dd, J = 10.2, 7.0 Hz), 3.56 (2H, s), 3.76 (1H, dd, J = 5.3, 1.4 Hz). ^{13}C NMR (100 MHz, DMSO-d_6): δ 26.1, 26.6, 27.9, 29.4, 32.9, 40.4, 51.6, 56.9, 61.4, 197.3, 200.0, 212.0. HR-ESI-MS *m/z*. Calcd for $C_{14}H_{20}O_3$\{[M + H]$^+$\}: 236.3110. Found: 236.3108. Elem. Anal. Calcd for $C_{14}H_{20}O_3$: C, 71.16; H, 8.53; O, 20.31. Found: C, 71.15; H, 8.54; O, 20.32%.

*Methyl 2-oxo-3-(3-oxobutanoyl)cyclopentane-1-carboxylate (compound **3g**)*. Orange-yellow oily liquid; yield 89.7%. ^{1}H NMR (400 MHz, DMSO-d_6): δ 1.85−2.33 (7H), 1.95 (dd, J = 13.8, 5.5 Hz), 2.03 (dd, J = 14.4, 5.4 Hz), 2.16 (dd, J = 13.8, 1.4 Hz), 2.15 (s), 2.23 (dd, J = 14.4, 1.4 Hz), 3.50−3.87 (7H, 3.56 (s), 3.66 (dd, J = 7.5, 7.0 Hz), 3.72 (s), 3.79 (dd, J = 5.3, 1.4 Hz). ^{13}C NMR (100 MHz, DMSO-d_6): δ 25.8, 27.2, 29.4, 52.2, 55.1, 56.9, 61.2, 170.9, 197.3, 200.0, 207.1. HR-ESI-MS *m/z*. Calcd for $C_{11}H_{14}O_5$\{[M + H]$^+$\}: 226.2280. Found: 226.2278. Elem. Anal. Calcd for $C_{11}H_{14}O_5$: C, 58.40; H, 6.24; O, 35.36. Found: C, 58.41; H, 6.25; O, 35.35%.

*Ethyl 2-oxo-3-(3-oxobutanoyl)cyclopentane-1-carboxylate (compound **3h**)*. Orange-yellow oily liquid; yield 88.1%. ^{1}H NMR (400 MHz, DMSO-d_6): δ 1.15 (3H, s), 1.85−2.28 (7H), 1.96 (dd, J = 13.8, 5.5 Hz), 2.06 (dd, J = 14.4, 5.4 Hz), 2.17 (dd, J = 13.8, 1.4 Hz), 2.19 (dd, J = 14.4, 1.4 Hz), 2.165 (s), 3.56 (2H, s), 3.60−3.86 (2H, 3.67 (dd, J = 7.5, 7.0 Hz), 3.80 (dd, J = 5.3, 1.4 Hz), 4.16 (2H, q, J = 7.1 Hz), ^{13}C NMR (100 MHz, DMSO-d_6): δ14.7, 27.2, 27.6, 29.4, 55.9, 56.9, 61.1, 61.8, 171.3, 197.3, 200.0, 207.1. HR-ESI-MS *m/z*. Calcd for $C_{12}H_{16}O_5$\{[M + H]$^+$\}: 240.2550. Found: 240.2548. Elem. Anal. Calcd for $C_{12}H_{16}O_5$: C, 59.99; H, 6.71; O, 33.30. Found: C, 59.96; H, 6.73; O, 33.31%.

*1-(3-Acetyl-2-oxocyclopentyl)butane-1,3-dione (compound **3i**)*. Orange-yellow oily liquid; yield 83.1%. ^{1}H NMR (400 MHz, DMSO-d_6): δ 1.92−2.28 (10H), 2.05 (dd, J = 14.0, 5.4 Hz), 2.12 (dd, J = 13.3, 5.5 Hz), 2.15 (dd, J = 13.3, 1.4 Hz), 2.17 (s), 2.20 (dd, J = 14.0, 1.4 Hz), 3.56 (4H, s), 3.63 (1H, dd, J = 6.9, 1.8 Hz), 3.72 (1H, dd, J = 9.3, 5.5 Hz). ^{13}C NMR (100 MHz, DMSO-d_6): δ 27.1, 27.7, 29.4, 30.0, 56.9, 61.1, 61.8, 197.3, 200.0, 202.6, 207.5. HR-ESI-MS *m/z*. Calcd for $C_{11}H_{14}O_4$\{[M + H]$^+$\}: 210.2290. Found: 210.2297. Elem. Anal. Calcd for $C_{11}H_{14}O_4$: C, 62.85; H, 6.71; O, 30.44. Found: C, 62.83; H, 6.72; O, 30.45%.

*Methyl 2-(3-oxo-4-(3-oxobutanoyl)-2-pentylcyclopentyl)acetate (compound **3j**)*. Orange-yellow oily liquid; yield 84.5%. ^{1}H NMR (400 MHz, DMSO-d_6): δ 0.88 (3H, s), 1.15−1.38 (6H), 1.22 (t, J = 6.5 Hz), 1.26 (h, J = 6.5 Hz), 1.29 (tt, J = 6.7, 6.5 Hz), 1.62 (2H, dd, J = 6.7, 4.7 Hz), 2.06−2.43 (6H, 2.16 (dd, J = 14.7, 9.3 Hz), 2.15 (s), 2.23 (tt, J = 14.7, 5.5 Hz), 2.34 (dd, J = 9.3, 5.0 Hz), 2.45−2.73 (3H), 2.56 (d, J = 5.0 Hz), 2.65 (dd, J = 6.9, 4.7 Hz), 3.56 (2H, s), 3.66 (4H, s), 3.72 (1H, dd, J = 9.3, 5.5 Hz). ^{13}C NMR (100 MHz, DMSO-d_6): δ 14.0, 23.2, 27.9, 28.3, 29.4, 31.5, 33.0, 33.9, 37.7, 51.9, 54.3, 56.9, 60.4, 173.1, 196.8, 200.0, 212.3. HR-ESI-MS *m/z*. Calcd for $C_{17}H_{26}O_5$\{[M + H]$^+$\}: 310.3900. Found: 310.3896. Elem. Anal. Calcd for $C_{17}H_{26}O_5$: C, 65.78; H, 8.44; O, 25.77. Found: C, 65.77; H, 8.45; O, 25.78%.

*3-Methyl-5-(3-oxobutanoyl) cyclopentane-1, 2-dione (compound **3k**)*. Orange-yellow oily liquid; yield 87.2%. ^{1}H NMR (400 MHz, DMSO-d_6): δ 1.22 (3H, s), 2.11−2.43 (5H), 2.15 (s), 2.24 (dd, J = 10.8, 6.7 Hz), 2.35 (dd, J = 10.8, 6.4 Hz)), 3.06 (1H, dd, J = 7.5, 6.6 Hz), 3.53 (2H, s), 3.91 (1H, dd, J = 8.3, 6.4 Hz). ^{13}C NMR (100 MHz, DMSO-d_6): δ 15.0, 29.3, 34.1, 39.2, 56.9, 62.3, 196.7, 200.0, 200.4, 209.0. HR-ESI-MS *m/z*. Calcd for $C_{10}H_{12}O_4$\{[M + H]$^+$\}:196.2020. Found: 196.2017. Elem. Anal. Calcd for $C_{10}H_{12}O_4$: C, 61.22; H, 6.17; O, 32.62. Found: C, 61.23; H, 6.18; O, 32.60%.

*4-Oxo-3-(3-oxobutanoyl)cyclopentane-1, 2-dicarboxylic acid (compound **3l**.* Orange-yellow oily liquid; yield 79.2%. ^{1}H NMR (400 MHz, DMSO-d_6): δ 2.15 (3H, s), 2.68 (1H, dd, J = 17.8, 6.9 Hz), 2.93 (1H, dd, J = 17.8, 7.6 Hz), 3.40−3.68 (4H, 3.51 (dd, J = 8.1, 6.9 Hz), 3.56 (s), 3.63 (dd, J = 8.1, 6.9 Hz), 3.85 (1H, d, J = 6.9 Hz). ^{13}C NMR (100 MHz, DMSO-d_6): δ 29.4, 41.2, 42.7, 48.1, 58.0, 59.6, 175.9, 176.4, 197.9, 200.0, 210.3. HR-ESI-MS *m/z*. Calcd for $C_{11}H_{12}O_7$\{[M + H]$^+$\}: 256.2100. Found. 256.2098. Elem. Anal. Calcd for $C_{11}H_{12}O_7$: C, 51.57; H, 4.72; O, 43.71. Found: C, 51.58; H, 4.72; O, 43.73%.

4.2. Biological Activity Experiment. *4.2.1. In Vitro Activity. 4.2.1.1. Detection of Inhibition Ratio of RAW 264.7 Cells.* Cells were divided into normal group, LPS group (Lipoid A), LPS+DMSO group, LPS+ positive drug group (methotrexate, 1 μM), LPS+each compounds group (each compound was set at three concentrations of 1, 10, and 100 μM). After cells were fully attached to the wall, the liquid in the wells was discarded. The same amount of medium was added to the normal group. The other groups were added to 1 μg/mL LPS, and the corresponding final concentrations of the compounds (the drugs that were not easily dissolved could be solubilized by DMSO). Culturing continued for 48 h; then, the liquids in the wells were discarded. Then, 200 μL of complete medium and 20 μL of CCK8 (Sigma-Aldrich) solution were added. Cells were cultured in a cell incubator for 3−4 h. The OD value was measured by a microplate detector at the wavelength of 450 nm. Inhibition rate = (OD value of normal group cells − OD value of drug administration group cells)/(OD value of normal group cells), and its IC_{50} value was calculated.

4.2.1.2. Detection of Inflammatory Factor Levels in RAW 264.7 Cells. Cells were divided into normal group, LPS group, LPS+DMSO group, LPS+positive drug group (methotrexate, 1 μM), LPS+each compounds group (each compounds were set at three concentrations of 1, 10, and 100 μM). After cells were fully attached to the wall, the liquids in the wells were discarded. The same amount of medium was added to the normal group. To the other groups were added 1 μg/mL LPS and the corresponding final concentrations of the compounds (the drugs that were not easily dissolved could be solubilized by DMSO). Culturing was continued for 48 h, cell supernatant was collected, and the levels for inflammatory factors IL-1β, IL-6, and TNF-α in each group were detected.

4.2.2. In Vivo Activity. 4.2.2.1. Determination of Rheumatoid Arthritis Induced by CIA in Rats. Mice and rats used in the animal experiment were purchased from Weitong Lihua Co. (China), License No. SCXK 2019-0001 and were raised on ordinary feed at a temperature of 20−26 °C and humidity of 40−70%. After 7 days for adaptive feeding, the tail roots of all rats were injected with type II collagen plus Complete Fredrin's Adjuvant (CFA, SIGMA, USA) emulsifier. Rats was immunized with 0.1 mL for emulsion of type II collagen (2 mg/mL) and

https://doi.org/10.1021/acsomega.4c02344
ACS Omega 2024, 9, 36232−36241

CFA with subcutaneous injection at 1.5 cm distal from the tail base. After 7 days, the rat rheumatoid arthritis was induced by subcutaneous enhanced injection into the foot plantar. Fourteen days after secondary injection, normal group, model group, methotrexate group, and compounds group were randomly selected. After successful modeling, rats in each group were given the corresponding drug orally, once a day, for a consecutive 15 days, with 100 and 50 mg/kg. Control group and model group were given normal saline. After the treatment, the paw was photographed and the paw volume was measured. Then each group of rats was killed, the serum of each group was collected, and ELISA was used to measure levels for TNF-α and IL-1β.

4.3. Experiment of Action Mechanism. *4.3.1. Protein Expressions for Inflammatory Factors TLR4, TNF-α, and NF-κB of RAW264.7 Cells Being Determined by Immunofluorescence Method.* Cells were divided into normal group, model group, methotrexate group, compound group and incubated for 24 h. The RAW264.7 cells were LPS-induced (1 μg/mL, Lipoid A) for 24 h, and 1 μM methotrexate and 1 μM target compound were added to other groups except normal group and model group, respectively. Continuing the intervention for 24 h, fluids in the pores were discarded and washed twice with 0.01 M PBS. After, they were fixed with 4% cells fixative for 45 min and treated with 0.25% Triton-100 for 15 min. And then they were closed with 5% BSA for 10 min, and rabbit antimouse TLR4 or TNF-α or NF-κB primary antibody diluent (1:100) was added. Incubation occurred overnight in 4 °C against light, and then liquids were discarded and the samples were washed with 0.01 M PBS for 5 times. FITC-labeled goat antirabbit secondary antibody diluent (1:400) was added, and samples were incubated at 37 °C against light for 30 min, after which the medium was discarded. After rinsing with 0.01 M PBS for 4 times, DAPI diluent (1:800) was added and the samples were incubated at room temperature and protected from light for 10 min; the solution was discarded and samples were rinsed with 0.01 M PBS for 3 times. Fluorescence detection was performed by confocal laser microscopy, and the average fluorescence intensity for the cells was used to indicate the relative expression levels for TLR4, TNF-α, and NF-κB proteins.

4.3.2. Protein Expressions for Inflammatory Factors TLR4, TNF-α, and NF-κB of RAW264.7 Cells Being Determined by Western Blot. Cells were divided into normal group, model group, methotrexate group, and compound group and incubated for 24 h. The RAW264.7 cells were LPS-induced (1 μg/mL, Lipoid A) for 24 h, and 1 μM methotrexate and 1 μM target compound were added to other groups except normal group and model group, respectively. After intervention continued for 24 h, liquids in the holes were discarded, and RIPA cells lysate containing 1% protease inhibition PMSF were added. The cell lysate was cracked on ice for 3−4 h and centrifuged at 12000 rpm of 15 min. The supernatant was taken and stored in a refrigerator at −80 °C for later use. Expression levels for TLR4, TNF-α, and NF-κB were measured by Western blot.

4.3.3. mRNA Expression for Inflammatory Factors TLR4, TNF-α, and NF-κB of RAW264.7 Cells Being Determined by RT-PCR. Cells were divided into normal group, model group, methotrexate group, and compound group and incubated for 24 h. The RAW264.7 cells were LPS-induced (1 μg/mL, Lipoid A) for 24 h, and 1 μM methotrexate and 1 μM target compound were added to other groups except normal group and model group, respectively. After intervention continued for 24 h, fluid in the hole was discarded and cells were treated with Trizol reagent on ice for 1−2 h. Supernatants were collected and stored in a refrigerator at −80 °C for later use. mRNA expression levels for TLR4, TNF-α, and NF-κB were measured by RT-PCR (Eppendorf, Realplex2).

4.4. Pharmacokinetics. The SD rats (6−8 weeks, male) were purchased from JH Laboratory Animal Co., Qualification No. SCXK (SH) 2022-0009 (20220009001365), and placed in an environmentally controlled breeding room with free access to water and food. Compound **3k** was dissolved in 10% DMSO + 10% solutool HS15 + 80% (20% HP-β-CD saline) to prepare a drug delivery solution. After a 20 mg/kg amount via foot dorsal vein injection, blood samples were collected at 0.08, 0.25, 0.5, 1, 2, 4, 6, 8, 12, and 24 h after intravenous administration. With 100 mg/kg via oral gavage, the blood was collected at 0.08, 0.25, 0.5, 1, 2, 4, 6, 8, 12, and 24 h after oral administration. About 150 μL of blood was collected from the jugular vein at each time point, placed on wet ice, and centrifuged at 2000g for 5 min (4 °C) within 15 min of sampling. After centrifugation, 5 μL of the supernatant solution was taken for LC-MS/MS (SCIEX, Triple Quad 7500) .

4.5. Molecular Docking Simulation. The structures of the ligands were drawn by Chemdraw, and their 3D structures were preprocessed by LigPrep using OPLS3 force field.[37−40] The ionization states of the ligand were determined via epik at pH = 7.0 ± 2.0. The crystallographic structure for TLR4 was collected from the protein data bank (PDB entry: 3FXI), which was then utilized for molecular docking. Prior to docking, the ligands were preprocessed by the protein preparation wizard module in maestro before generating a docking grid. The ligand docking between the target molecule and TLR4 was obtained using standard precision (SP) docking. The remaining parameters were kept at their default setup.[41]

4.6. Statistical Methods. SPSS 22.0 was used for analysis. Experimental data were expressed by mean ± standard deviation, and one-way ANOVA analyses were used to compare data between groups, with $p < 0.05$ indicating the statistically significant differences and $p < 0.01$ indicating the statistically significant differences.

AUTHOR INFORMATION

Corresponding Authors

Shiyang Zhou − *Chongqing Chemical Industry Vocational College, Chongqing 401228, China; School of Biological and Chemical Engineering, Chongqing University of Education, Chongqing 400067, China; Chongqing Academy of Traditional Chinese Medicine, Chongqing 400065, China; Key Laboratory of Tropical Medicinal Plant Chemistry of Hainan Province, Hainan Normal University, Haikou 571158, China; School of Pharmaceutical Sciences, Chongqing University, Chongqing 401331, China;* orcid.org/0000-0002-1100-8863; Email: zhoushiyang520@126.com

Weiwei Xue − *School of Pharmaceutical Sciences, Chongqing University, Chongqing 401331, China;* orcid.org/0000-0002-3285-0574; Email: xueww@cqu.edu.cn

Jun Tan − *School of Biological and Chemical Engineering, Chongqing University of Education, Chongqing 400067, China*; Email: tanjun@cque.edu.cn

Complete contact information is available at: https://pubs.acs.org/10.1021/acsomega.4c02344

https://doi.org/10.1021/acsomega.4c02344
ACS Omega 2024, 9, 36232−36241

Notes

Animal Ethics Statement: Mice and rats used in the animal experiment were purchased from Weitong Lihua Co. (China), License No. SCXK 2019-0001, and were raised on ordinary feed at a temperature of 20−26 °C and humidity of 40−70%. All animal procedures were performed in accordance with the guidelines of care and used for laboratory animals for "Chongqing University of Education" and the experiment was approved by the animal ethics committee for "Chongqing University of Education" under No. 20230413.
The authors declare no competing financial interest.

■ ACKNOWLEDGMENTS

The project was sponsored by the Science and Technology Research Program of Chongqing Municipal Education Commission of China (KJZD-K202204502 and KJQN20230450), the Chongqing Natural Science Foundation Innovation Development Joint Fund (CSTB2022NSCQ-LZX0053), the Chongqing Natural Science Foundation project (CSTB2024NSCQ-MSX0273), and Key Laboratory of Tropical Medicinal Resource Chemistry of Ministry of Education, Hainan Normal University (RDZH2023004).

■ REFERENCES

(1) Zhou, S.; Zou, H.; Chen, G.; Huang, G. Synthesis and biological activities of chemical drugs for the treatment anti-rheumatoid. *Top. Curr. Chem.* **2019**, *377*, 28.
(2) Zhai, K. F.; Duan, H.; Luo, L.; Cao, W. G.; Han, F. K.; Shan, L. L.; Fang, X. M. Protective effects of paeonol on inflammatory response in IL-1beta-induced human fibroblast-like synoviocytes and rheumatoid arthritis progression via modulating NF-kappaB pathway. *Inflammopharmacology* **2017**, *25*, 523−532.
(3) (3.) Zhai, K. F.; Duan, H.; Chen, Y.; Khan, G. J.; Cao, W. G.; Gao, G. Z.; Shan, L. L.; Wei, Z. J. Apoptosis effects of imperatorin on synoviocytes in rheumatoid arthritis through mitochondrial/caspase-mediated pathways. *Food Funct.* **2018**, *9*, 2070−2079.
(4) Dai, D. F.; Chen, T.; Szeto, H.; Nieves-Cintron, M.; Kutyavin, V.; Santana, L. F.; Rabinovitch, P. S. Mitochondrial targeted antioxidant Peptide ameliorates hypertensive cardiomyopathy. *J. Am. Coll. Cardiol.* **2011**, *58*, 73−82.
(5) Zhang, T.; Ikejima, T.; Li, L.; Wu, R.; Yuan, X.; Zhao, J.; Wang, Y.; Peng, S. Impairment of mitochondrial biogenesis and dynamics involved in isoniazid-induced apoptosis of HepG2 cells was alleviated by p38 MAPK pathway. *Front. Pharm.* **2017**, *8*, 753.
(6) Liu, Z.; Wang, F.; Zhou, Z. W.; Xia, H. C.; Wang, X. Y.; Yang, Y. X.; He, Z. X.; Sun, T.; Zhou, S. F. Alisertib induces G2/M arrest, apoptosis, and autophagy via PI3K/Akt/mTOR- and p38 MAPK-mediated pathways in human glioblastoma cells. *Am. J. Transl. Res.* **2017**, *9*, 845−873.
(7) Zhai, K; Gao, G; Cao, W; Zhao, L; Fang, X; Duan, H. Simultaneous HPLC determination of four active compounds in fengshiding capsules, a chinese medicine. *Indian J. Pharm. Sci.* **2014**, *76*, 445−449.
(8) Yan, C.; Kong, D.; Ge, D.; Zhang, Y.; Zhang, X.; Su, C.; Cao, X. Mitomycin C induces apoptosis in rheumatoid arthritis fibroblast-like synoviocytes via a mitochondrial-mediated pathway. *Cell. Physiol. Biochem.* **2015**, *35*, 1125−1136.
(9) Shang, C. H.; Zhang, Q. Q.; Zhou, J. H. Oridonin inhibits cell proliferation and induces apoptosis in rheumatoid arthritis fibroblast-like synoviocytes. *Inflammation* **2016**, *39*, 873−880.
(10) Huang, M.; Zeng, S.; Qiu, Q.; Xiao, Y.; Shi, M.; Zou, Y.; Yang, X.; Xu, H.; Liang, L. Niclosamide induces apoptosis in human rheumatoid arthritis fibroblast-like synoviocytes. *Int. Immunopharmacol.* **2016**, *31*, 45−49.
(11) Nakatani, Y.; Kobe, A.; Kuriya, M.; Hiroki, Y.; Yahagi, T.; Sakakibara, I.; Matsuzaki, K.; Amano, T. Neuroprotective effect of liquiritin as an antioxidant via an increase in glucose-6-phosphate dehydrogenase expression on B65 neuroblastoma cells. *Eur. J. Pharmacol.* **2017**, *815*, 381−390.
(12) Cheel, J.; Antwerpen, P. V.; Tumova, L.; Onofre, G.; Vokurkova, D.; Zouaoui-Boudjeltia, K.; Vanhaeverbeek, M.; Neve, J. Free radical-scavenging, antioxidant and immunostimulating effects of a licorice infusion (Glycyrrhiza glabra L.). *Food Chem.* **2010**, *122*, 508−517.
(13) Jia, S. L.; Wu, X. L.; Li, X. X.; Dai, X. L.; Gao, Z. L.; Lu, Z.; Zheng, Q. S.; Sun, Y. X. Neuroprotective effects of liquiritin on cognitive deficits induced by soluble amyloid-β1−42 oligomers injected into the hippocampus. *J. Asian Nat. Prod. Res.* **2016**, *18*, 1186−1199.
(14) Zou, S.; Wang, C.; Cui, Z.; Guo, P.; Meng, Q.; Shi, X.; Gao, Y.; Yang, G.; Han, Z. β-Elemene induces apoptosis of human rheumatoid arthritis fibroblast-like synoviocytes via reactive oxygen species-dependent activation of p38 mitogen-activated protein kinase. *Pharmacol. Rep.* **2016**, *68*, 7−11.
(15) Wang, J.; Yuan, L.; Xiao, H.; Xiao, C.; Wang, Y.; Liu, X. Momordin Ic induces HepG2 cell apoptosis through MAPK and PI3K/Akt-mediated mitochondrial pathways. *Apoptosis* **2013**, *18*, 751−65.
(16) Yan, J.; Chen, Y.; He, C.; Yang, Z. Z; Lu, C.; Chen, X. S. Andrographolide induces cell cycle arrest and apoptosis in human rheumatoid arthritis fibroblast-like synoviocytes. *Cell Biol. Toxicol* **2012**, *28*, 47−56.
(17) Zhang, Y.; Zhang, L.; Zhang, Y.; Xu, J. J.; Sun, L. L.; Li, S. Z. The protective role of liquiritin in high fructose-induced myocardial fibrosis via inhibiting NF-kappaB and MAPK signaling pathway. *Biomed. Pharmacother.* **2016**, *84*, 1337−1349.
(18) Zhou, Y.; Ho, W. S. Combination of liquiritin, isoliquiritin and isoliquirigenin induce apoptotic cell death through upregulating p53 and p21 in the A549 non-small cell lung cancer cells. *Oncol. Rep.* **2014**, *31*, 298−304.
(19) Wei, F.; Jiang, X.; Gao, H. Y.; Gao, S. H. Liquiritin induces apoptosis and autophagy in cisplatin (DDP)-resistant gastric cancer cells in vitro and xenograft nude mice in vivo. *Int. J. Oncol.* **2017**, *51*, 1383−1394.
(20) Wang, X. H.; Jiang, S. M.; Sun, Q. W. Effects of berberine on human rheumatoid arthritis fibroblast-like synoviocytes. *Exp. Biol. Med.* **2011**, *236*, 859−66.
(21) Rath, S.; Das, L.; Kokate, S. B.; Ghosh, N.; Dixit, P.; Rout, N.; Singh, S. P.; Chattopadhyay, S.; Ashktorab, H.; Smoot, D. T.; Swamy, M. M.; Kundu, T. K.; Crowe, S. E.; Bhattacharyya, A. Inhibition of histone/lysine acetyltransferase activity kills CoCl2-treated and hypoxia-exposed gastric cancer cells and reduces their invasiveness. *Int. J. Biochem. Cell Biol.* **2017**, *82*, 28−40.
(22) Wang, J.; Zhang, Y. S.; Thakur, K.; Hussain, S. S.; Zhang, J. G.; Xiao, G. R.; Wei, Z. J. Licochalcone A from licorice root, an inhibitor of human hepatoma cell growth via induction of cell apoptosis and cell cycle arrest. *Food Chem. Toxicol.* **2018**, *120*, 407−417.
(23) Zhai, K.; Duan, H.; Cui, C.; Cao, Y.; Si, J.; Yang, H.; Wang, Y.; Cao, W.; Gao, G.; Wei, Z. Liquiritin from Glycyrrhiza uralensis Attenuating Rheumatoid Arthritis via Reducing Inflammation, Suppressing Angiogenesis, and Inhibiting MAPK Signaling Pathway. *J. Agric. Food Chem.* **2019**, *67*, 2856−2864.
(24) Zhai, K.; Wang, W.; Zheng, M.; Khan, G. J.; Wang, Q.; Chang, J.; Dong, Z.; Zhang, X.; Duan, H.; Gong, Z.; Cao, H. Protective effects of Isodon Suzhouensis extract and glaucocalyxin A on chronic obstructive pulmonary disease through SOCS3-JAKs/STATs pathway. *Food Front.* **2023**, *4*, 511−523.
(25) Wu, Y.; Zhang, S.; Yin, Q.; Lei, M.; Wang, Q.; Chen, W.; Luo, T.; Zhou, P.; Ji, C. α-Mangostin Inhibited M1 Polarization of Macrophages/Monocytes in Antigen-Induced Arthritis Mice by Up-Regulating Silent Information Regulator 1 and Peroxisome Proliferators-Activated Receptor γ Simultaneously. *Drug Des. Dev. Ther.* **2023**, *17*, 563−577.
(26) Bartok, B.; Firestein, G. S. Fibroblast-like synoviocytes: key effector cells in rheumatoid arthritis. *Immunol. Rev.* **2010**, *233*, 233−255.
(27) Yin, L.; Guan, E.; Zhang, Y.; Shu, Z.; Wang, B.; Wu, X.; Chen, J.; Liu, J.; Fu, X.; Sun, W.; Liu, M. Chemical profile and antiinflammatory

https://doi.org/10.1021/acsomega.4c02344
ACS Omega 2024, 9, 36232−36241

activity of total flavonoids from Glycyrrhiza Uralensis Fisch. *Iran. J. Pharm. Res.* **2018**, *17*, 726−734.
(28) Cao, L. J.; Hou, Z. Y.; Li, H. D.; et al. The ethanol extract of licorice (Glycyrrhiza uralensis) protects against triptolide-induced oxidative stress through activation of Nrf2. *Evid. Based Complement. Altern. Med.* **2017**, *2017*, 2752389.
(29) Lim, C.; Lim, S.; Lee, B.; Kim, B.; Cho, S. Licorice pretreatment protects against brain damage induced by middle cerebral artery occlusion in mice. *J. Med. Food* **2018**, *21*, 474−480.
(30) Zhai, K. F.; Duan, H.; Khan, G. J.; Xu, H.; Han, F. K.; Cao, W. G.; Gao, G. Z.; Shan, L. L.; Wei, Z. J. Salicin from Alangium chinense ameliorates rheumatoid arthritis by modulating the Nrf2-HO-1-ROS pathways. *J. Agric. Food Chem.* **2018**, *66*, 6073−6082.
(31) Ayeka, P. A.; Bian, Y.; Githaiga, P. M.; Zhao, Y. The immunomodulatory activities of licorice polysaccharides (Glycyrrhiza uralensis Fisch.) in CT 26 tumor-bearing mice. *BMC Complementary Altern. Med.* **2017**, *17*, 536.
(32) Zhai, K. F.; Zheng, J. R.; Tang, Y. M.; Li, F.; Lv, Y. N.; Zhang, Y. Y.; Gao, Z.; Qi, J.; Yu, B. Y.; Kou, J. P. The saponin D39 blocks dissociation of non-muscular myosin heavy chain IIA from TNF receptor 2, suppressing tissue factor expression and venous thrombosis. *Br. J. Pharmacol.* **2017**, *174*, 2818−2831.
(33) Zhou, X.; Zheng, C.; Zhang, Y.; Zhang, X.; Song, X.; Xu, W.; Chen, G. Guaiane-Type Sesquiterpenoids from Fissistigma oldhamii Inhibit the Proliferation of Synoviocytes. *Planta Med.* **2017**, *83*, 217−223.
(34) Zhou, S.; Jiang, W.; Chen, G.; Huang, G. Design and Synthesis of Novel Double-Ring Conjugated Enones as Potent Anti-rheumatoid Arthritis Agents. *ACS Omega* **2022**, *7*, 44065−44077.
(35) Zhou, S.; Huang, G.; Chen, G.; Liu, J. Synthesis, activity and mechanism for double-ring conjugated enones. *Bioorg. Med. Chem. Lett.* **2021**, *49*, 128315.
(36) Zhou, S.; Zou, H.; Huang, G.; Zhou, X.; Chen, G.; Huang, S. Design, synthesis and anti-rheumatoid arthritis evaluation of double-ring conjugated enones. *Bioorg. Chem.* **2021**, *109*, 104701.
(37) Jain, A. N. Surflex: Fully automatic flexible molecular docking using a molecular similarity-based search engine. *J. Med. Chem.* **2003**, *46*, 499−511.
(38) Kim, H. M.; Park, B. S.; Kim, J. I.; Kim, S. E.; Lee, J.; Oh, S. C.; Enkhbayar, P.; Matsushima, N.; Lee, H.; Yoo, O. J.; Lee, J. O. Crystal structure of the TLR4-MD-2 complex with bound endotoxin antagonist eritoran. *Cell* **2007**, *130*, 906−917.
(39) Cochet, F.; Facchini, F. A.; Zaffaroni, L.; Billod, J. M.; Coelho, H.; Holgado, A.; Braun, H.; Beyaert, R.; Jerala, R.; Jimenez-Barbero, J.; Martin-Santamaria, S.; Peri, F. Novel carboxylate-based glycolipids: TLR4 antagonism, MD-2 binding and self-assembly properties. *Sci. Rep.* **2019**, *9*, 919.
(40) Wang, S.; Chen, G.; Kayser, M. M.; Iwaki, H.; Lau, P. C.; Hasegawa, Y. Baeyer-Villiger oxidations catalyzed by engineered microorganisms: Enantioselective synthesis of δ-valerolactones with functionalized chains. *Can. J. Chem.* **2002**, *80*, 613−621.
(41) Ogura, T.; Usuki, T. Total synthesis of acerogenins E, G and K, and centrolobol. *Tetrahedron* **2013**, *69*, 2807−2815.
(42) Wang, W.; Zhou, S.; Jiang, W.; Chen, G. Design, synthesis and anti-rheumatoid arthritis activity of target TLR4 inhibitors. *Bioorg. Med. Chem.* **2024**, *97*, 117539.

https://doi.org/10.1021/acsomega.4c02344
ACS Omega 2024, 9, 36232−36241